

Path Integral Monte Carlo study of phonons in the bcc phase of ^4He

V.Sorkin,* E. Polturak, and Joan Adler

Physics Department, Technion - Israel Institute of Technology, Haifa, Israel, 32000

(Dated: December 2, 2024)

Using Path Integral Monte Carlo and the Maximum Entropy method, we calculate the dynamic structure factor of solid ^4He in the bcc phase at a finite temperature of $T = 1.6$ K and a molar volume of 21 cm^3 . Both the single-phonon contribution to the dynamic structure factor and the total dynamic structure factor are evaluated. From the dynamic structure factor, we obtain the phonon dispersion relations along the main crystalline directions, [001], [011] and [111]. We calculated both the longitudinal and transverse phonon branches. For the latter, no previous simulations exist. We discuss the differences between dispersion relations resulting from the single-phonon part vs. the total dynamic structure factor. In addition, we evaluated the formation energy of a vacancy.

PACS numbers:

I. INTRODUCTION

Solid helium, the well-known example of a quantum solid, continues to be a subject of interest to theorists and experimentalists alike. Most recently, reports have appeared indicating a possible existence of a "supersolid" in the hcp phase¹. In the bcc phase, an optical-like excitation branch was discovered^{2,3}, in addition to the 3 acoustic phonon branches which are all one would expect to observe in a mono-atomic cubic solid. Solid helium is characterized by the large zero-point motion and significant short-range correlation of its atoms. These effects make the theoretical description of the solid very difficult. The self-consistent phonon (SCP) method^{4,5} developed over the years to treat this problem, takes into account the high anharmonicity and short-range correlations in order to calculate the dynamical properties of solid helium. The predictions of the SCP agree with experiment especially well in the fcc and hcp solid phases. In the low-density bcc phase, the agreement between the theory and experiment is less satisfactory, in particular regarding the transverse phonons along the [110] direction.⁶ The SCP theory is a variational perturbative theory, and is applied for zero-temperature calculations.⁴ As a complementary approach to the SCP, numerical simulations were performed over the years. Boninsegni and Ceperley used Path Integral Monte Carlo (PIMC) to calculate the phonon spectrum of liquid ^4He . Chester et al. used the Shadow Wave Function approach to obtain the spectra of longitudinal phonons in hcp and bcc ^4He at zero temperature. Following along this line, we decided to apply Quantum Monte Carlo simulations to study the dynamics of atoms in solid helium. We use Path Integral Monte Carlo (PIMC)¹⁰⁻¹², a non-perturbative numerical method, which allows in principle simulations of quantum systems without any assumptions beyond the Schrödinger equation. The two body interatomic He-He potential¹³ is the only input in the PIMC simulations. The novel features in our work include the calculation of the transversal phonon branches in bcc ^4He at finite temperature of 1.6 K where this phase is stable. Our particular interest in the transverse phonons stems from

the work of Gov⁶, who proposed that the new excitation branch^{2,3} is a result of coupling of transverse phonons to additional degrees of freedom, unique to a quantum solid. In addition, we repeated our calculations of the phonon spectra in the presence of point defects (vacancy).

We describe details of our simulations in Sec. II. In Sec. III we present the results of our calculations, and summarize them in Sec. IV.

II. METHOD

The PIMC method used in our simulations, based on the formulation of quantum mechanics in terms of path integrals, was described in detail by Ceperley¹⁰. In this method, a quantum system of particles is mapped onto a classical model of interacting "ring polymers", whose elements, "beads or time-slices", are connected by "springs". The method provides a direct statistical evaluation of quantum canonical averages. In addition to static properties of the system, dynamical properties could be also extracted from PIMC simulations.¹⁰

The object of our study is phonon spectrum, which can be extracted from the dynamic structure factor, $S(\mathbf{Q}, \omega)$. $S(\mathbf{Q}, \omega)$ describes the correlations of density fluctuations, and it is defined as

$$S(\mathbf{Q}, \omega) = \frac{1}{2\pi n} \int_{-\infty}^{+\infty} dt e^{i\omega t} \langle \rho_{\mathbf{Q}}(t) \rho_{-\mathbf{Q}}(0) \rangle, \quad (1)$$

where $\hbar\mathbf{Q}$ and $\hbar\omega$ are the momentum and energy (we take $\hbar = 1$), and $\rho_{\mathbf{Q}}$ is the Fourier transform of the density of the solid, and n is the number density. $S(\mathbf{Q}, \omega)$ is usually expressed in terms of phonons, by writing $S(\mathbf{Q}, \omega)$ as a sum of terms involving the excitation of a single phonon, $S_1(\mathbf{Q}, \omega)$, a pair of phonons, $S_2(\mathbf{Q}, \omega)$ and higher order terms which also include an interference between the different terms.^{4,5} In most of our simulations we calculated the $S_1(\mathbf{Q}, \omega)$ term. Some calculation of $S(\mathbf{Q}, \omega)$ were also performed, and will be discussed below.

Taking the instantaneous position $\mathbf{r}(l, t)$ of atom l as the lattice point \mathbf{R}_l plus a displacement $\mathbf{u}(l, t) =$

$\mathbf{r}(l, t) - \mathbf{R}(l, t)$, we rewrite $S(\mathbf{Q}, \omega)$ in terms of these displacements. The one-phonon contribution is then given by⁴

$$S_1(\mathbf{Q}, \omega) = d^2(\mathbf{Q}) \sum_l e^{i\mathbf{Q}(\mathbf{R}_l - \mathbf{R}_0)} \langle [\mathbf{Q}\mathbf{u}(l, t)][\mathbf{Q}\mathbf{u}(l, 0)] \rangle, \quad (2)$$

where $d(\mathbf{Q}) = \langle \exp(-\frac{1}{2}(\mathbf{u}\mathbf{Q})^2) \rangle$ is the Debye-Waller factor.

The displacement $\mathbf{u}(l, t)$ can be expressed using the phonon operators $A_{\mathbf{q}, \lambda}(t)$ ^{15,16}

$$\mathbf{u}(l, t) = \sum_{\mathbf{q}, \lambda} A_{\mathbf{q}, \lambda}(t) \exp(-i\mathbf{q}\mathbf{R}_l) \hat{\mathbf{e}}_\lambda, \quad (3)$$

where \mathbf{q} is the phonon wave-vector, λ is the phonon branch index, and $\hat{\mathbf{e}}_\lambda$ are polarization vectors, chosen along the directions [001], [011] and [111]. Using $A_{\mathbf{q}, \lambda}(t)$, the one-phonon term $S_1(\mathbf{Q}, \omega)$ for a specific phonon branch is rewritten as⁴

$$S_1 = \sum_{\mathbf{q}, \lambda} \int_{-\infty}^{+\infty} \langle A_{\mathbf{q}, \lambda}(t) A_{-\mathbf{q}, \lambda}(0) \rangle \Delta_{\mathbf{Q}, \mathbf{q} - \mathbf{G}} d^2[\mathbf{Q}\hat{\mathbf{e}}_\lambda]^2 e^{i\omega t} dt, \quad (4)$$

where $\Delta_{\mathbf{Q}, \mathbf{q} - \mathbf{G}}$ is the delta function, and \mathbf{G} is a reciprocal lattice vector. We use \mathbf{Q} , which lies inside the first Brillouin zone and parallel to one of e_λ . Therefore, $S_1(\mathbf{Q}, \omega) = S_1(\mathbf{q}, \omega)$, and $S_1(\mathbf{q}, \omega)$ is given by

$$S_1 = \sum_\lambda S_{1, \lambda} = \sum_\lambda \int_{-\infty}^{+\infty} e^{i\omega t} F_{\mathbf{q}, \lambda}(t) dt, \quad (5)$$

and

$$F_{\mathbf{q}, \lambda}(t) = \int_{-\infty}^{+\infty} e^{-i\omega t} S_{1, \lambda}(\mathbf{q}, \omega) d\omega \quad (6)$$

is the intermediate scattering function.

We cannot follow directly the dynamics of helium atoms in real time using the Quantum Monte Carlo method. Nevertheless we can extract information about the dynamics by means of analytical continuation of $F_{\mathbf{q}, \lambda}(t)$ to the complex plane⁷ $t \rightarrow i\tau$. Using imaginary-time, we obtain

$$F_{\mathbf{q}, \lambda}(\tau) = \int_0^{+\infty} S_{1, \lambda}(\mathbf{q}, \omega) \left(e^{-\omega\tau} + e^{-\omega(\beta - \tau)} \right) d\omega \quad (7)$$

where $F_{\mathbf{q}, \lambda}(\tau)$ is the intermediate scattering function, $\beta = 1/kT$.

In our simulations, we sampled the displacement $\mathbf{u}(l, \tau)$ for each "time-slice" τ of the l -th atom represented by a "ring polymer", and calculated $A_{\mathbf{q}, \lambda}(\tau)$ by performing spatial Fourier transformation

$$A_{\mathbf{q}, \lambda}(\tau) = \sum_l \hat{\mathbf{e}}_\lambda \mathbf{u}(l, \tau) \exp(i\mathbf{q}\mathbf{R}_l) \quad (8)$$

Using (8), $F_{\mathbf{q}}$ is obtained as a quantum canonical average of the product $\langle A_{\mathbf{q}, \lambda}(\tau) A_{-\mathbf{q}, \lambda}(0) \rangle$ in equilibrium.

In order to calculate $S_{1, \lambda}(\mathbf{q}, \omega)$ from Eq.(7), we need to perform an inverse Laplace transformation. Performing the inversion is a difficult numerical problem,^{10,17} because of the inherent statistical uncertainty of noisy PIMC data. The noise rules out an unambiguous reconstruction of the $S_{1, \lambda}(\mathbf{q}, \omega)$. The best available method to circumvent this problem is to apply the Maximum Entropy (MaxEnt)^{17,18} method that makes the Laplace inversion better conditioned.

The MaxEnt method yields a dynamic scattering function, $S_{1, \lambda}(\mathbf{q}, \omega)$ which satisfies Eq. (7) and at the same time maximizes the conditional probability imposed by our knowledge of the system. (9) That can be done if some properties of $S_{1, \lambda}(\mathbf{q}, \omega)$ are known. Some examples of such properties: the dynamic scattering factor is a non - negative function, and has certain asymptotic behavior at small and large $[\omega]$. In the MaxEnt method the probability to observe of a given dynamic scattering function is given by

$$P(S_1 | \langle F_\tau \rangle) \sim \exp\left(-\frac{1}{2}\chi^2 + \alpha S_{ent}\right) \quad (9)$$

where $P(S_1 | \langle F_\tau \rangle)$ is probability to observe $S_1(\omega)$ for given set of sampled QMC data $\langle F_\tau \rangle$ (intermediate scattering function (6)), χ^2 is the likelihood, α is a parameter and S_{ent} entropy¹⁷. To simplify our notation, from now on we denote by $S_1(\omega)$ the one-phonon dynamic structure $S_{1, \lambda}(\mathbf{q}, \omega)$ for a given \mathbf{q} and λ , and omit the explicit dependence on \mathbf{q} and λ . Similarly, we replace $F_{\mathbf{q}, \lambda}(\tau)$ by F_τ .

The likelihood χ^2 is given by

$$\chi^2 = \sum_{\tau, \tau'} (K_{\tau', \omega} S_1 - \langle F_{\tau'} \rangle)^T C_{\tau', \tau}^{-1} (K_{\tau, \omega} S_1 - \langle F_\tau \rangle) \quad (10)$$

where the kernel $K_{\tau, \omega}$ is defined as

$$K_{\tau, \omega} = \exp(-\tau\omega) + \exp(-(\beta - \omega)\tau) \quad (11)$$

The covariance matrix, $C_{\tau, \tau'}$, describes the correlation between the different time slices τ for a given atom ("ring" polymer). This matrix is defined as

$$C_{\tau, \tau'} = \langle F_\tau F_{\tau'} \rangle - \langle F_\tau \rangle \langle F_{\tau'} \rangle, \quad (12)$$

where $\langle F_\tau \rangle$ is obtained as an average over all atoms at a given time slice τ . Because F_τ is periodic as one goes around the polymer⁷, the summation on τ is done for $\tau = 1, M/2$, where M is the total number of time-slices in a "polymer ring".

The entropy term S_{ent} is added to χ^2 in order to make the reconstruction procedure better conditioned^{10,17}. We remark here that in some Quantum MC simulations only the diagonal elements of $C_{\tau, \tau'}$ are taken into account¹⁷, but here we use all the elements, because $\langle F_\tau \rangle$ at different τ are correlated with each other.

Although χ^2 measures how close does any form of $S_1(\omega)$ approximates the solution of Eq. (7), one cannot determine $S_1(\omega)$ reliably from PIMC using χ^2 alone.^{10,17} To do so, one needs to add the entropy term S_{ent} to χ^2 in (9) to make the reconstruction procedure better conditioned. The entropy term is given by

$$S_{ent}(\omega) = - \int_0^\infty d\omega \left(S_1(\omega) \ln \frac{S_1(\omega)}{m(\omega)} + S_1(\omega) - m(\omega) \right) \quad (13)$$

where $m(\omega)$ includes our prior knowledge about the properties of $S_1(\omega)$, examples of which were given above. The simplest choice of $S_1(\omega)$ is the flat model, in which $m(\omega) = \text{const}$ for a selected range of frequencies and zero otherwise. We took the cutoff frequency corresponding to an energy of 100K. This flat model is used as an input for the most part of our simulations. In addition, we used a “self-consistent” model where the output of a previous MaxEnt reconstruction is used as input for the next MaxEnt reconstruction in an iterative fashion^{7,10} The flat model is taken for the initial iteration. Finally, we also tried $m(\omega)$ with Gaussian and Lorentzian shape, with peaks given by the SCP theory and experiment. As explained below, the outcome is not very sensitive to the choice of $m(\omega)$ provided the PIMC data are of good quality.

Finally, we discuss the parameter α in (9). The magnitude of this parameter controls the relative weight of the PIMC data vs. the entropy term in the determination of $S_1(\omega_1)$. There are different strategies to obtain α . In our simulations we used both the “classical” MaxEnt method¹⁷ and random walk sampling.⁷ The “classical” MaxEnt method picks the best value of α , while random walk sampling calculates a distribution of α , $\pi(\alpha)$. Next, for each value of α we calculate $S_1(\omega)$. The final $S_1(\omega)$ is obtained as a weighted average over α . We found that when the collected PIMC data is of good quality, the distribution $\pi(\alpha)$ becomes sharply peaked and symmetric, and the phonon spectra obtained by means of “classical” MaxEnt and random walk are almost the same. Good quality data are characterized by absence of correlation between sequential PIMC steps and by small statistical errors.

The MaxEnt method assumes that the distribution of the sampled F_τ is Gaussian.¹⁷ We re-block¹⁷ the sampled values of F_τ in order to reduce the correlations and to make the distribution as close as possible to a Gaussian, with zero third (skewness) and fourth (kurtosis) moments.

The criterion determining the minimum number of measurements comes from the properties of the covariance matrix $C_{\tau,\tau'}$. If there are not enough blocks of data the covariance matrix becomes pathological.¹⁷ Therefore, the number of blocks must be larger than the number of time slices in a “ring” polymer. In our simulations, each atoms is represented by a “ring” polymer with 64 time slices. We collected at least the 300 blocks in each simulation run. We found that at least 10000 measurements

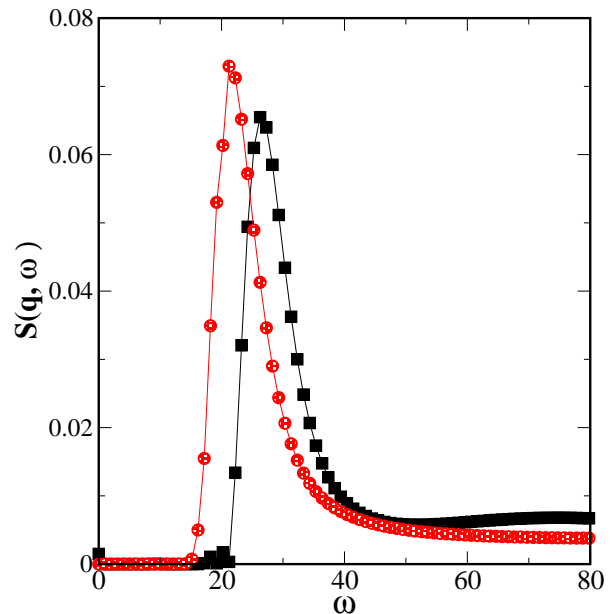


FIG. 1: Longitudinal component of the dynamic structure factor for $q = 0.83$ r.l.u. along the [100] direction: single phonon contribution (circles), and total structure factor (squares). The lines are guide to the eye.

were required in order to obtain 300 blocks of good quality data.

Statistical errors were estimated by running the PIMC simulations 10 times, with different initial conditions. After each run, $S(\mathbf{q}, \omega)$ was extracted using the MaxEnt method. The phonon energy for a given \mathbf{q} was then calculated by averaging the positions of the peak of $S(\mathbf{q}, \omega)$ over the set of the simulation runs. The error bars of each point shown in the figures below represent the standard deviation.

III. RESULTS

In the simulations we used samples containing between 128 and 432 atoms. This allowed us to calculate $S(\mathbf{q}, \omega)$ for values of q between 0.17 and 1 in relative lattice units (r.l.u. = $2\pi/a$, where a is the lattice parameter). The number density was set to $\rho = 0.02854$ ($1/A^3$) and the temperature was $T = 1.6$ K. A perfect bcc lattice was chosen as the initial configuration. A typical example of the calculated dynamic structure factor is shown in Fig.1. The figure shows both the single phonon contribution $S_1(\mathbf{q}, \omega)$ and the total $S(\mathbf{q}, \omega)$ for a longitudinal phonon along the [001] direction. To illustrate the difference between $S_1(\mathbf{q}, \omega)$ and $S(\mathbf{q}, \omega)$, we chose to show the results for \mathbf{q} close to the boundary of the Brillouin zone. This difference is discussed below.

The calculated longitudinal and transverse phonon spectra of solid ${}^4\text{He}$ in the bcc phase along the main crystal directions ([001], [111] and [011]) are shown in

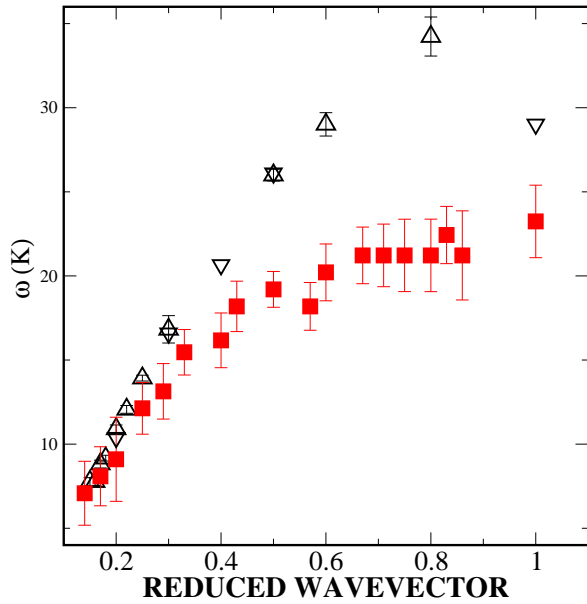


FIG. 2: Calculated dispersion relation of the L[001] phonon branch (squares) using $S_1(\mathbf{q}, \omega)$. Experimental data are from^{19,21} (triangles up) and from³ (triangles down).

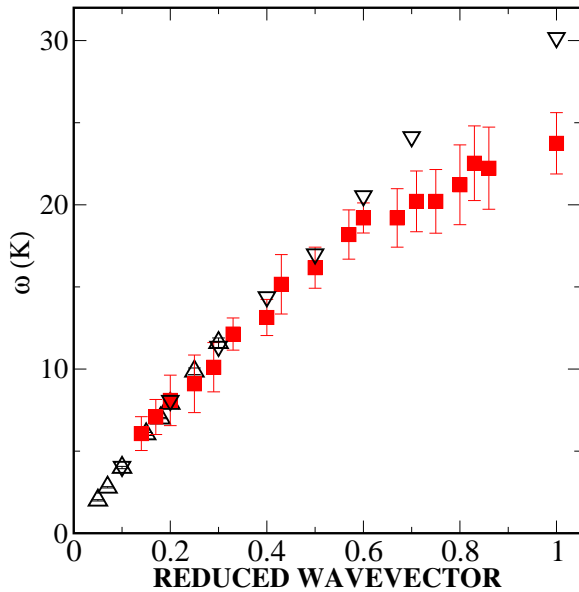


FIG. 3: Calculated dispersion relation of the T[001] phonon branch (squares) using $S_1(\mathbf{q}, \omega)$. Experimental data are from^{19,21} (triangles up) and from³ (triangles down).

Figs. 2 - 7. We compare our results with the experimental data measured by inelastic neutron scattering from bcc ^4He with a molar volume of 21.1 cm^3 at $T = 1.6 \text{ K}$, by Osgood et al,¹⁹⁻²¹ and by Markovitch et al.³

As expected, the agreement between our simulations of $S_1(\omega, \mathbf{q})$ and experiment is very good at small \mathbf{q} , where one-phonon excitation is the most significant contribution to $S(\omega, \mathbf{q})$. As \mathbf{q} increases, higher order processes be-

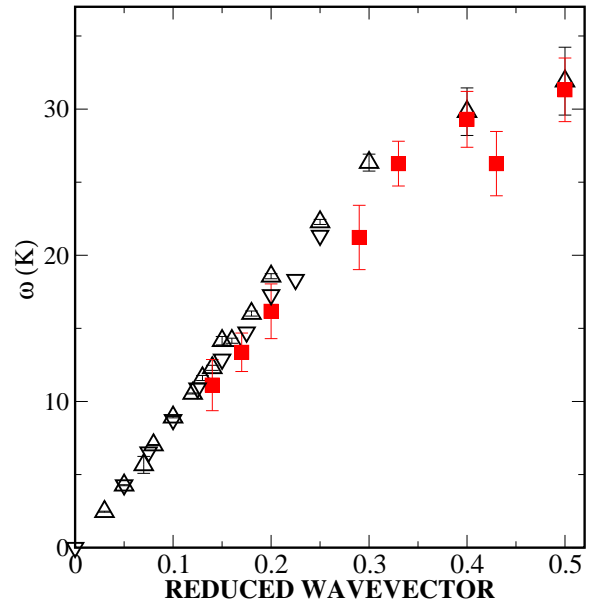


FIG. 4: Calculated dispersion relation of the L[011] phonon branch (squares) using $S_1(\mathbf{q}, \omega)$. Experimental data are from^{19,21} (triangles up) and from³ (triangles down).

come significant, and the calculated values deviate from the experimental data, especially along [001] and [111]. In the case of longitudinal phonons, it is possible to calculate their energies using the total $S(\omega, \mathbf{q})$ obtained directly from Eq. (1) instead of just the single phonon contribution. The dispersion relations calculated with $S(\omega, \mathbf{q})$ are shown in Figs. 8 and 9. It is evident that using the total scattering function improves the agreement with experiment at large \mathbf{q} , especially for the [111] direction.

We point out that the calculated phonon branches $T_1(110)$, $T_2(110)$ and $L(110)$ show good fit to the experimental data. Our results were obtained with the two body potential, which takes the He atoms as point particles. Gov et al.⁶ suggested that one needs to go beyond this approximation to obtain the $T_1(110)$ phonon branch in good agreement with experiment. Gov's approach also predicts the new excitation branch observed recently². Although the calculated $T_1(110)$ branch is in agreement with experiment without any additional assumptions, we were not able to see the new excitation in our simulations. Experimentally, this excitation is about an order of magnitude less intense than a phonon. It is best observed in scattering experiments done with very small $\mathbf{q} \leq 0.1 \text{ r.l.u.}^3$. Both these factors make it very difficult to search for this excitation in simulations. Whether it can be found in this approach remains an open question.

In addition to experimental results, our simulations can be also compared with those of Galli and Reatto⁹, who used the Shadow Wave Function approach to calculate the longitudinal phonon branches of bcc ^4He . This comparison is shown in Fig.10

The overall agreement seems to be good. Recent ex-

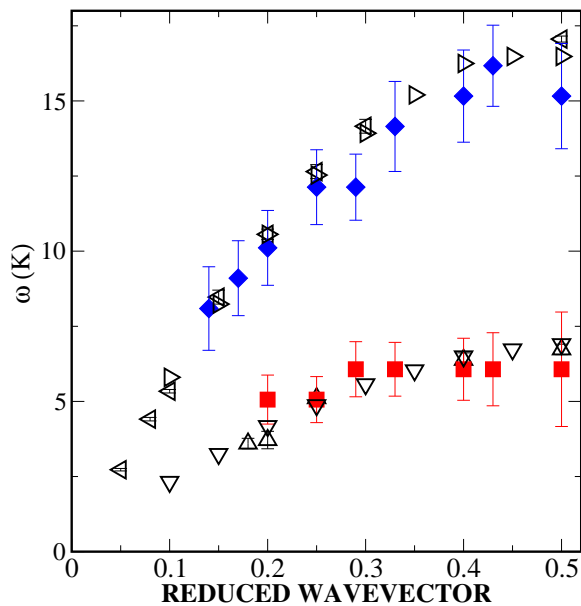


FIG. 5: Calculated dispersion relations of transverse phonon branches along [011] using $S_1(\mathbf{q}, \omega)$. Calculated values are shown for the T_1 branch (squares) and T_2 branch (diamonds). Experimental data are from^{19,21} (T_1 -triangles up, T_2 -triangles left) and from³ (T_1 -triangles down, T_2 -triangles right).

perimental work¹ revived the interest in point defects, such as vacancies. It is therefore interesting to examine the influence of vacancies on the properties of the solid. We repeated our calculation of the phonon branches in the presence of 0.23% vacancies (1 atom of 432). Within the statistical error bars, we found no difference between the phonon energies with or without vacancies. Galli and Reatto⁹ found that vacancies lower the energies of the phonons close to the boundary of the Brillouin zone. However, in their simulation they used a concentration of vacancies of 0.8%, so that the cumulative effect may be larger. In addition, we calculated the vacancy formation energy, ΔE_v , according to Pederiva et al.²²

$$\Delta E_v = (E(N-1, \rho) - E(N, \rho))(N-1), \quad (14)$$

where $E(N, \rho)$ is the total energy of N atoms. The energy $E(N, \rho)$ was calculated for a perfect crystal, while $E(N-1, \rho)$ was calculated after removing one atom. The density of two systems was kept the same by adjusting the lattice parameter.

Values of ΔE_v calculated using the PIMC, Shadow Wave Function (SWF)¹⁴ and Shadow Path Integral Ground State (SPIGS)⁹ methods are summarized in Table I. There is no generally accepted experimental value²³ of ΔE_v . According to NMR studies^{24,7} the energy of vacancy formation in the bcc phase is $\Delta E_v = 6.5 \pm 0.2(\text{K})$, while X-ray studies²⁶ suggest that $\Delta E_v = 9 \pm 1(\text{K})$. We comment here that the calculated values of ΔE_v are significantly smaller than 14K, the energy of the new excitation observed by Markovitch et

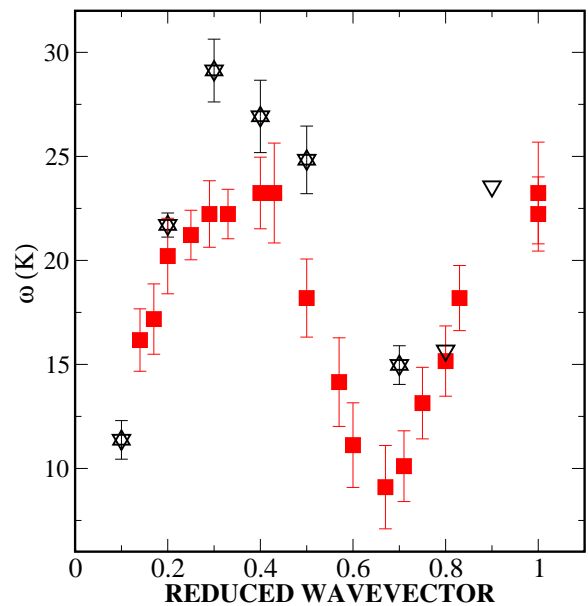


FIG. 6: Calculated dispersion relation of the L[111] phonon branch (squares) using $S_1(\mathbf{q}, \omega)$. Experimental data are from^{19,21} (triangles up) and from³ (triangles down).

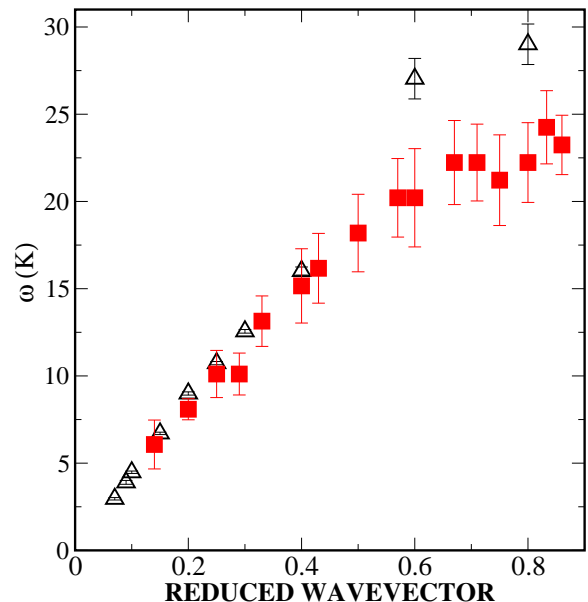


FIG. 7: Calculated dispersion relation of the T[111] phonon branch (squares) using $S_1(\mathbf{q}, \omega)$. Experimental data are from^{19,21} (triangles up) and from³ (triangles down).

al.^{2,3}. Hence, this new excitation does not seem to be a simple vacancy.

IV. CONCLUSIONS

We calculated the dynamic structure factor for solid helium in the bcc phase using the PIMC simulations and

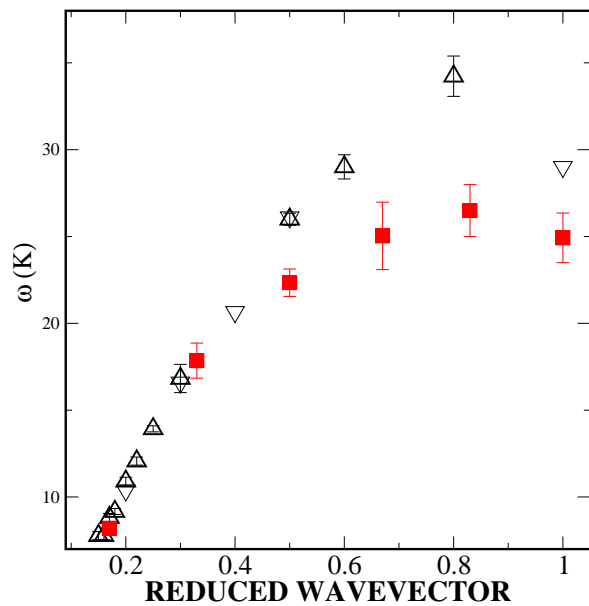


FIG. 8: Calculated dispersion relation of the L[001] phonon branch (squares) using $S(\omega, \mathbf{q})$. Experimental data are from^{19,21} (triangles up) and from³(triangles down).

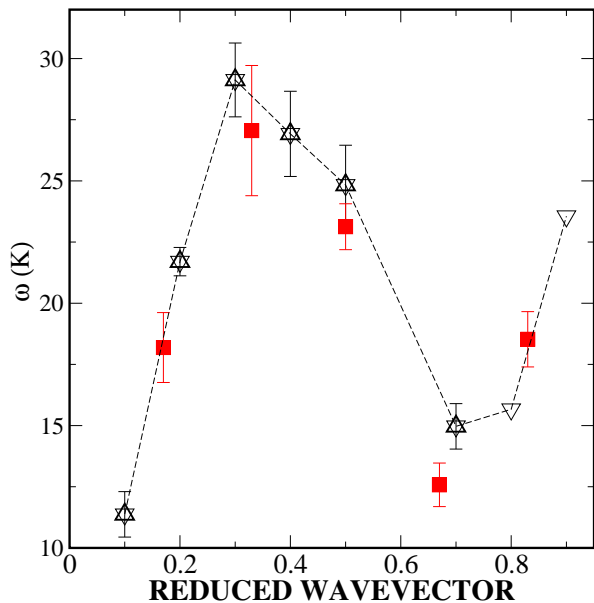


FIG. 9: Calculated dispersion relation of the L[111] phonon branch (squares) using $S(\omega, \mathbf{q})$. Experimental data are from^{19,21} (triangles up) and from³(triangles down). The dashed line to guide the eye.

the MaxEnt method. Path integral Monte Carlo was used to calculate the intermediate scattering function in the imaginary time from which the dynamic structure factor was inferred with the MaxEnt method. In reconstruction of the dynamic structure factor we found that MaxEnt does not resolve all the real structure observed experimentally. The MaxEnt favors the “smooth”

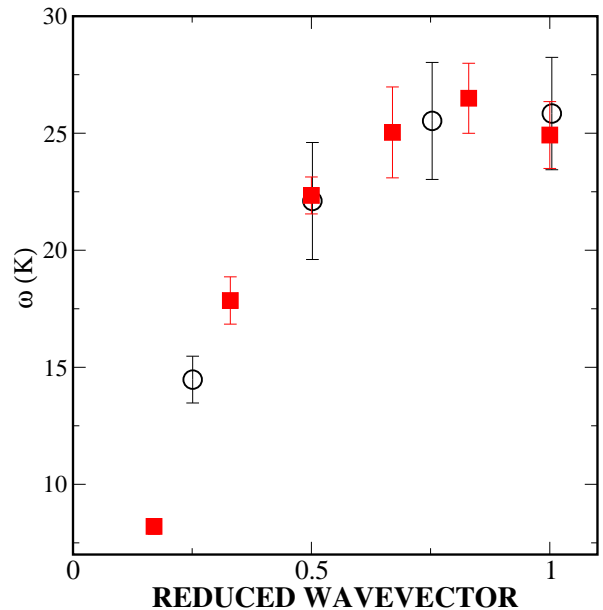


FIG. 10: A comparison of dispersion relations of the L[001] phonon branch obtained in the present work using $S(\omega, \mathbf{q})$ (squares), with the same relation calculated by means of the Shadow Wave Function technique⁹ (circles).

TABLE I: Calculated energy of formation of a vacancy, ΔE_v , for bcc solid ${}^4\text{He}$. N is the number of atoms used in each of the simulations.

source	method	density ($1/\text{Å}^3$)	N	ΔE_v (K)
this work	PIMC	0.02854	128	10.57 ± 0.38
this work	PIMC	0.02854	250	9.96 ± 0.89
ref. ¹⁴	SWF	0.02854	128	8.08 ± 2.76
ref. ¹⁴	SWF	0.02854	250	6.69 ± 3.86
ref. ⁹	SWF	0.02898	128	8.9 ± 0.3
ref. ⁹	SPIGS	0.02898	128	8.0 ± 1.3

Gaussian-like spectral functions. In the calculated dynamic structure factors we did not observe the small secondary peak along the [110] direction, which corresponds to the new excitations, predicted by Gov et al.⁶ and observed experimentally².

We extracted the longitudinal and transverse phonon branches from the one-phonon dynamic structure factor. At small \mathbf{q} , where the one-phonon excitation is the most significant contribution to the dynamic structure factor, the agreement between our simulations and experiment is very good. At large \mathbf{q} , multi-phonon scattering and interference effects⁴ becomes important. Consequently, the position of the peak of in the $S_1(\mathbf{q}, \omega)$ does not correspond to the position of the peak in the $S(\mathbf{q}, \omega)$, and the phonon energies calculated from $S_1(\mathbf{q}, \omega)$ are too low. If $S(\mathbf{q}, \omega)$ is used instead of $S_1(\mathbf{q}, \omega)$, the agreement is noticeably improved. We repeated the simulations in the presence of 0.23% of vacancies, and found no significant differences in the phonon dispersion relations. In addition, the formation energy of a vacancy was calculated.

Acknowledgments

We wish to thank D. Ceperley for many helpful discussions and for providing us with UPI9CD PIMC code. We

are grateful to N. Gov, O. Pelleg and S. Meni for their contribution to this work. This study was supported in part by the Israel Science Foundation and by the Technion VPR fund for promotion of research.

-
- * Electronic address: phsorkin@techunix.technion.ac.il; URL: <http://phycomp.technion.ac.il/~phsorkin/index.html>
- ¹ E. Kim and M. H. W. Chan, *Science*, **305**, 1941, (2004).
 - ² T. Markovitch, E. Polturak, J. Bossy, and E. Farhi, *Phys. Rev. Lett.*, **88**, 195301, (2002).
 - ³ T. Markovitz, *Inelastic-Neutron Scattering from bcc ⁴He*, PhD. Thesis, Haifa, Technion, (2001).
 - ⁴ H. R. Glyde, *Excitations in Liquid and Solid Helium*, Clarendon Press, Oxford, (1994).
 - ⁵ H. Horner, *J. Low. Temp. Phys.* **8**, 511, (1972).
 - ⁶ N. Gov and E. Polturak, *Phys. Rev. B*, **60**, 1019, (1999).
 - ⁷ M. Boninsegni and D. M. Ceperley, *J. Low. Temp. Phys.* **104**, 336, (1996).
 - ¹⁴ B. Chaudhuri, F. Pederiva, and G. V. Chester, *Phys. Rev. B.*, **60**, 3721, (1999).
 - ⁹ D. E. Galli and L. Reatto, *J. Low. Temp. Phys.*, **134**, 121, (2004).
 - ¹⁰ D. M. Ceperley, *Rev. Mod. Phys.*, **67**, 279, (1995)
 - ¹¹ K. Ohno, K. Esfarjam, Y. Kawazoe, *Computational Material Science; From Ab Initio to Monte Carlo Methods*, Springer, Berlin, 1999.
 - ¹² B. Bernu and D. M. Ceperley, in *Quantum Simulations of Complex Many-Body Systems: From Theory to Algorithms*, NIC Series **10**, Julich, 2002.
 - ¹³ R. A. Aziz, A. R. Janzen, and M. R. Moldover, *Phys. Rev. Let.* **74**, 1586 (1995).
 - ¹⁴ M. Born and K. Huang, *Dynamical theory of crystal lattices*, Clarendon Press, Oxford, (1954).
 - ¹⁵ P. Bruesch, *Phonons, theory and experiments I: lattice dynamics and models of inter atomic forces*, Berlin, Springer, (1982).
 - ¹⁷ M. Jarrell and J. E. Gubernatis, *Phys. Rep.*, **269**, 133, (1996).
 - ¹⁸ J. E. Gubernatis, M. Jarrell, R. N. Silver, and D. S. Sivia *Phys. Rev. B* **44**, 6011, (1991).
 - ¹⁹ E. B. Osgood, V. J. Minkiewicz, T. A. Kitchens, and G. Shirane, *Phys. Rev. A* **5**, 1537 (1972).
 - ²⁰ E. B. Osgood, V. J. Minkiewicz, T. A. Kitchens, and G. Shirane, *Phys. Rev. A* **6**, 526 (1972).
 - ²¹ V. J. Minkiewicz, T. A. Kitchens, G. Shirane, and E. B. Osgood, *Phys. Rev. A* **8**, 1513 (1973).
 - ²² F. Pederiva, G. V. Chester, S. Fantoni, and L. Reatto, *Phys. Rev. B* **56**, 5909, (1997).
 - ²³ C. A. Burns and J. M. Goodkind, *J. Low. Temp. Phys.*, **95**, 695, (1994).
 - ²⁴ A. R. Allen, M. G. Richards, and G. Sharter, *J. Low. Temp. Phys.*, **47**, 289, (1982).
 - ²⁵ I. Schuster, E. Polturak, Y. Swirsky, E. J. Schmidt, and S. G. Lipson, *J. Low Temp. Phys.* **103**, 159, (1996).
 - ²⁶ B. A. Fraass, P. R. Granfors, and R. O. Simmons, *Phys. Rev. B.*, **39**, 124, (1989).